USING SHORT-PERIOD SURFACE WAVES TO MODEL SOURCE PHENOMENA

Heather Hooper[1], Howard J. Patton[2], Jessie L. Bonner[1], and Mark Leidig[1]

Weston Geophysical Corporation[1], Los Alamos National Laboratory[2]

Sponsored by National Nuclear Security Administration
Office of Nonproliferation Research and Engineering
Office of Defense Nuclear Nonproliferation

Contract No. DE-FG02-00ER83123

ABSTRACT

Nearfield and local seismograms of chemical explosions from 1) the Balapan depth of burial (DOB) experiment and 2) the Arizona source phenomenology experiment (SPE) provide an excellent opportunity to study the excitation of *Rg* waves for source effects. For the DOB experiment, *Rg* waves were identified using particle motion analysis and isolated from other arrivals using group velocity filtering. Fourier spectra were estimated, amplitude and phase information were processed, and path effects were removed. An *Rg* Q model and path-specific velocity models for phase corrections were developed for removal of path effects. Using a grid-search method, network-averaged source spectra were inverted to obtain source parameters for an axisymmetric source consisting of a monopole plus a compensated linear vector dipole (CLVD) or a horizontal tensile crack. The suite of observations, including ground-zero accelerograms and borehole logs, are best satisfied by models involving a CLVD with non-zero static moment. The CLVD source is related to tensile failure occurring at depths above the shot point, but a non-zero moment distinguishes this source from classical spallation source models. It appears to be more closely related to a conical source of block motions like the faulting source envisaged by Masse (1981). *Rg* source amplitudes are consistent with m_b(*Lg*) measurements at MAK, as would be expected if nearfield *Rg*-to-*S* scattering plays a role in generating *S*-waves seen at regional distances.

A new dataset recorded in September 2003 at a coal mine near Black Mesa, Arizona has allowed us to further examine the excitation of *Rg* from explosions in and below a topographic bench at the mine. A frequency-dependent attenuation model was developed and used to isolate source spectra and to generate radiation patterns. The source spectra for a set of nine explosions show that the one fully confined explosion scaled similarly to a Mueller-Murphy explosion with equivalent yield and depth of burial at most *Rg* frequencies. However, shots detonated at shallow depths that were not confined have frequency-dependent decoupling factors that vary from 2 to 10 at frequencies between 0.5 and 4 Hz when compared to theoretical scaling from a Mueller-Murphy source. Radiation patterns and spectral ratios from the explosions show increased energies and spectral ratios (factor of 1.5 increase) at azimuths behind the bench. Finally, spectral ratio plots show that detonating explosions with equivalent radiation patterns is a difficult task in the highly-fractured Black Mesa source medium.

OBJECTIVE

The objective of this research project is to improve nuclear monitoring efforts by developing an improved understanding of short-period surface waves generated by explosions. To accomplish this objective, we have created physically realistic models of short-period (0.2 to 12 second) surface wave generation from small chemical explosions and mine blast analogues. Additionally, we have worked to understand the propagation characteristics of these surface waves, possibly leading to an improved understanding of the physical mechanisms leading to the excitation of explosion-generated *Lg*.

RESEARCH ACCOMPLISHED

Rg Excitation by Underground Explosions: Insights from the Balapan DOB Experiment (Patton)

It has long been recognized that shallow sources excite *Rg* waves efficiently, but little is known about the mechanism(s) of *Rg* excitation by underground explosions. The excitation of *Rg* waves is of interest because of the role it may play in the generation of *Lg* waves and *Lg* coda from underground explosions. Gupta *et al.* (1992) proposed nearfield *Rg*-to-*S* scattering as a "transfer function" for converting energy radiated by underground explosions into *S* waves that become trapped in the crust and propagate to regional distances. Experimental support for this hypothesis comes from empirical studies (Gupta *et al.*, 1992; Myers *et al.*, 1999) and modeling studies (Patton and Taylor, 1995; Gupta *et al.*, 1997). A current limitation of modeling studies is that the source mechanism for *Rg* waves has to be assumed. Obtaining an improved understanding of the source of *Rg* waves is an important step towards building models of nearfield *Rg*-to-S scattering that can be tested against regional observations on a quantitative basis.

Explosions in the field are not simple monopole sources; rather, they are distributed in time and space, and emit non-spherical wave fields. Patton and Taylor (1995) proposed that the *Rg* excitation mechanism might involve a compensated linear vector dipole (Knopoff and Randall, 1970), where the CLVD is the elastodynamic equivalent of an inverted conical volume source with its apex at the detonation point. The medium inside the cone deforms and fails as a result of tensile stresses set up by the passage of the downgoing shock wave reflected off the free surface. Spallation, which usually involves shallow, poorly-coupling strata that open and close with no net displacement, is an example of such failure. Another example is that of driven block motions at depth, as envisioned by Masse (1981), which may have more significance for seismic wave generation, since it should allow for better coupling into the surrounding rock, and may involve permanent deformations.

Nearfield recordings of the 25-ton chemical explosions making up the DOB experiment at the Balapan test site, Semipalatinsk (Pearson *et al.*, 1997), offer a unique opportunity to investigate the excitation of *Rg* waves. Usable data were obtained from four nearfield stations for three of the depth of burial explosions.

Nearfield *Rg* Analysis

1) *Rg* waves were identified by (a) examining particle motions and (b) comparing observed arrival times with predictions based on the velocity models of Bonner *et al.* (2001).
2) *Rg* was extracted from the waveforms using the group-velocity filtering method of Landisman *et al.* (1969). This was necessary because the frequency content of the *P*, *S*, and *Rg* waves overlapped, and there wasn't enough time separation between the phases to do Fourier analysis on just the *Rg* signal.
3) The extracted *Rg* signals were Fourier transformed, and displacement spectra were calculated by dividing the amplitude and unwrapped phase spectra by *iw*. Noise spectra were also taken on a segment of coda the same length as the signal. Signal levels were usually well above the noise in the frequency band of interest.
4) Source spectra were calculated by correcting for the effects of amplitude attenuation and propagation phase delay using an *Rg* Q model and path-specific phase velocity models developed for that purpose.

Network spectra for three DOB explosions are shown in Figure 1, along with synthetic *Rg* spectra for a pure monopole source. The synthetic spectra were computed using the normal mode method of Saito (1967) for seismic moment M_o, determined using the scaling relationships for cavity radius and scalar moment of Denny and Johnson (1991; eqs. 39 and 41). For additional details of this study, both background and technical, see our extended abstract from the 25th Seismic Research Review (Bonner *et al*., 2003).

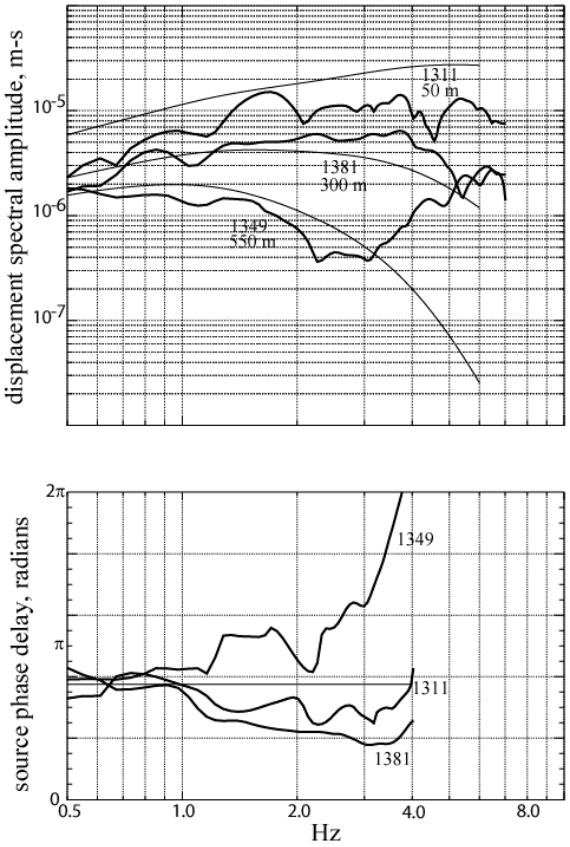

Figure 1. Network averaged *Rg* source spectra. (Top) Observed amplitude spectra (thick lines) and calculated amplitude spectra (thin lines) are for an equalization distance of 10 km. (Bottom) Observed phase delay spectra (thick lines) and the calculated spectrum (thin line) which applies to all three explosions.

Modelling Nearfield *Rg* Spectra

The next step was to model the nearfield *Rg* spectra for source effects using composite, axisymmetric sources. These sources consisted of a pure monopole linearly superposed with one of two secondary sources: either a CLVD or a horizontally-opening tensile crack. For practical and theoretical reasons, we chose to model network mean amplitude and phase spectra for each explosion. The model specifications included: (1) the centroid depth of the secondary source, (2) the source function of the secondary source, and (3) the M_o ratio between the secondary source and the monopole. The monopole M_o was determined by scaling the synthetic spectrum of the composite source to the observed amplitudes at low frequencies. The depth of the monopole was fixed to the centroid depth of the explosive package, and the source spectrum was assumed to be flat for the range of frequencies modeled based on the corner frequencies reported by Denny (1998).

The inversion was conducted by trial and error parameter search as follows:

1) The time history of the secondary source was fixed at a trial specification; we employed a von-Seggern-Blandford (1972) time history with two independent parameters: K (rise time) and B (overshoot);
2) A systematic search was conducted over centroid depth and M_o ratio on a 2-D grid;
3) At each grid point, the synthetic spectrum was scaled to match the observed amplitudes by least squares for frequencies of 0.5 - 1.5 Hz (0.8 - 1.5 Hz in the case of 1349); in doing so, the monopole M_o was determined;
4) Log amplitude and phase residuals were computed over specified frequency ranges: 0.8 - 6 Hz for amplitudes and 0.8 - 4 Hz for phase;
5) Residuals were contoured; the solution was taken to be the grid point with the minimum residual;
6) K and B were varied systematically and steps 2-5 were repeated.

The secondary source was delayed with respect to the explosion origin, where the delay was computed using the total transit time of a *P* wave emitted by the monopole source, reflected off the free surface with vertical incidence, and propagated down to the centroid depth of the secondary source. Thus the delay is solely a function of the

centroid depths and the Earth structure. The overall best solution was determined from the residuals as a function of K and B, using information from borehole logs and ground-zero (GZ) acceleration records for context.

Before discussing the results, we briefly review the salient features of *Rg* excitation by axisymmetric sources. The spectra in Figure 2 were computed keeping source function and source strength fixed while varying centroid depth. Each source type displays a unique *Rg* excitation. For a monopole, high frequency excitation systematically falls off as source depth increases. For a tensile crack, long-period excitation is weak in the upper 400 m. CLVD source spectra are more complicated due to the presence of spectral nulls related to source depth. Generally speaking, *Rg* excitation by the CLVD source can be as efficient as the monopole at low frequencies and less or more efficient at high frequencies depending on the respective source depths.

Phase spectra are identical for monopole and tensile crack sources and do not vary as a function of depth. On the other hand, *Rg* waves for a CLVD are 180° out of phase with respect to a monopole for frequencies less than the spectral null. Frequencies higher than the spectral null are in phase. Note that these results pertain to simultaneous sources with step function time history. The phasing will change for a secondary source delayed in time and with a different time history. Under those circumstances, superposition of monopole and secondary sources can lead to complicated interference patterns as a function of frequency.

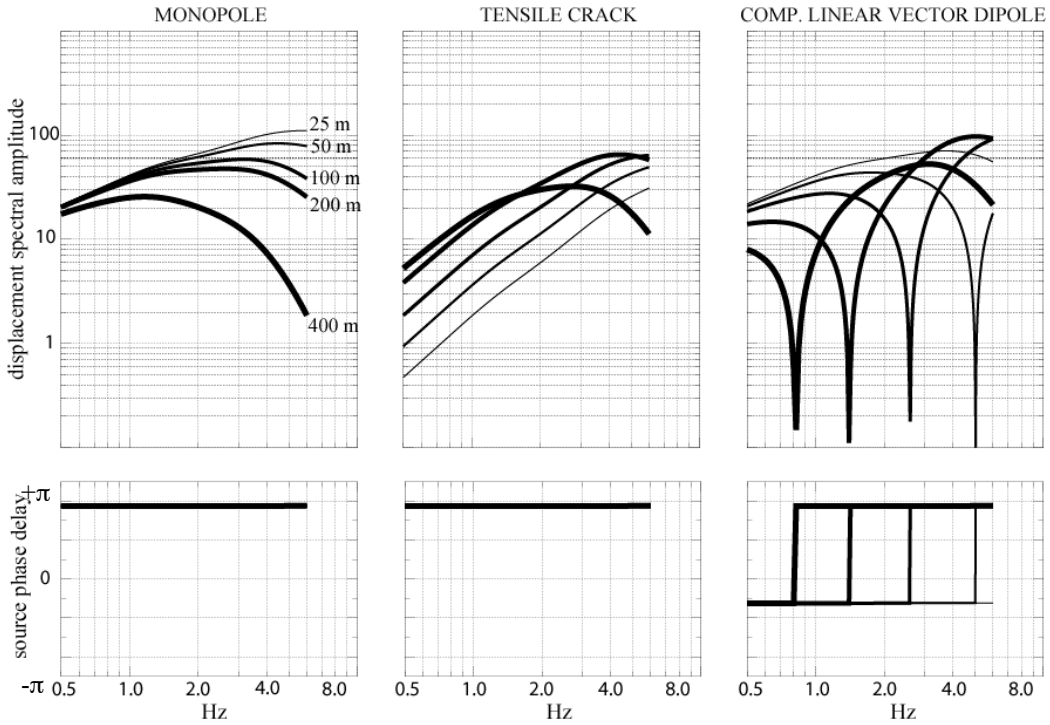

Figure 2. Synthetic *Rg* spectra for three sources with vertical axes of symmetry. All spectra were computed with a step function source time history. The vertical dipole moment Mzz was held fixed. (Left) The source description of a monopole explosion has equal moments along the diagonal of the moment tensor (M_{xx}, M_{yy}, M_{zz})=(1.0, 1.0, 1.0). (Center) The source description of a horizontal tensile crack is ($\lambda/(\lambda+2\mu)$, $\lambda/(\lambda+2\mu)$, 1.0). (Right) The source description of a CLVD with vertical axis of symmetry is (-0.5, -0.5, 1.0). Calculations are for centroid depths of 25, 50, 100, 200 and 400 m, where line thickness on the graph increases as depth increases. λ and μ are elastic constants.

Inversion results for 1349. The explosion in hole 1349 had a centroid depth of 535 m and a scaled depth of burial (SDOB) of ~1450 m/kt$^{1/3}$. Despite its depth, the free-surface acceleration records show that the medium over ground zero (GZ) spalled in response to the downgoing tensile wave. The depth of spall inferred from the time delay of the spall signal after the first arrival is remarkably deep, ~300 m or more, and borehole logs confirm the presence of layering with weak tensile strength at depths of ~340 m. The inversion results also favor an unusually deep secondary source of *Rg* waves. The solution with the overall minimum residual for a CLVD source is 250 m

deep with (K,B) of (100,10), while for a tensile crack source, it is 80 m deep with (K,B) of (100,1). The tensile crack centroid moves deeper as B increases. (Time history parameters were sampled at K = 1, 10, 100, 1000, 10000 and B = 1, 10, 100.) Both CLVD and tensile crack models fit the spectra well, and it is not possible to say which is in fact the true mechanism. Nevertheless, the behavior of the residuals for both models strongly suggests a link between the occurrence of tensile failure at depth and the excitation of *Rg* waves by a secondary source.

Inversion results for 1381. The explosion in hole 1381 had a centroid depth of 285 m and an SDOB of ~770 m/kt$^{1/3}$. Free-surface acceleration records show that the medium over GZ spalled, but in this case the spall occurred at shallow depths, which is more commonly the case for buried explosions. The time delay gives a depth of ~40 m, and borehole logs show a contact between overlying shales and basement rock at 41 m. The inversion results yield a centroid depth for a CLVD source consistent with a depth of 40 m and (K,B) of (1000,10). There are no physically meaningful solutions for a tensile crack. The rejection of all reasonable composite models involving a tensile crack model is due to the inability to match the spectral phase observations, which show phase advance relative to the phase spectrum predicted for a pure monopole (see Figure 2). Composite models involving a CLVD can predict phase advance because the source phase for a 40 m centroid depth is 180° out of phase with respect to a monopole for frequencies less than 7 Hz, and in addition there is a phase delay coming from the delayed origin time of the CLVD. Thus, the *Rg* observations for 1381 (and 1311) rule out a tensile crack mechanism, and we favor a CLVD mechanism for 1349 as well.

Inversion results for 1311. The explosion in hole 1311 had a centroid depth of 35 m and an SDOB of ~95 m/kt$^{1/3}$. It created a crater 40 m wide and roughly 5-10 m deep. The residuals for a CLVD source favor a very shallow centroid depth, and K greater than or equal to 100. The B value is not well resolved, however as B increases, the M_o ratio and the monopole M_o decrease, and almost all models with B greater than or equal to 10 have monopole M_o less than or equal to the monopole M_o estimated for 1381. These models contradict theoretical predictions that cavity size (hence M_o) should increase as rock strength diminishes due to lower overburden pressures (Glenn and Myers, 1997). Thus theory, coupled with the shallow depth of burial for 1311, argues for a larger M_o, hence a small value for B. A cratering source might be better modelled by time histories with little or no overshoot (B = 0) because there is no slap down (compaction) or gravitational reloading over GZ, as occurs in explosions with spall. (K,B) of the favored model is (100,1).

Summary Figure 3 shows time histories of the monopole and CLVD sources, as determined by Denny (1998) and the results of this study. Of significance are the static displacements associated with the CLVD source. The presence of statics may not be surprising for 1311 since cratering ejected material, and this could have resulted in elastic rebound over GZ. But 1381 and 1349 were spalling events, and the results for 1381 indicate statics associated in some way with tensile failure in the medium over the explosion. This finding contradicts conventional spall models (Stump, 1985; Day and McLaughlin, 1991) since they do not predict static M_o. Inversions assuming an impulse function gave large residuals for 1381, and all such models can be rejected; in the case of 1349, the results are equivocal, but favor a non-zero static M_o.

A CLVD force system with net M_o fits the source model proposed by Masse (1981) and could have important implications for the explosion source. While classical spall can be dismissed as a source of long-period Rayleigh waves (Day and McLaughlin, 1991), a CLVD source will radiate such waves with significant amplitudes if the static M_o is large enough (M_o ratio > 0.3). Long-period Rayleigh waves from monopole and CLVD sources will destructively interfere, canceling the amplitudes of waves emitted by the explosion. Such cancellation could affect measurements of explosion M_s, and, under extreme circumstances, the polarity of the resultant Rayleigh wave.

Finally, Figure 4 compares relative *Lg* amplitudes based on m_b(*Lg*) measured at station MAK with synthetic *Rg* spectra calculated for the preferred source models. The comparisons show very good agreement between the *Lg* amplitudes and the *Rg* source spectra for the composite monopole + CLVD source. Neither a monopole nor a CLVD source alone match the relative amplitudes. Thus, the composite source models are consistent with *Lg* waves generated by *Rg*-to-S scattering.

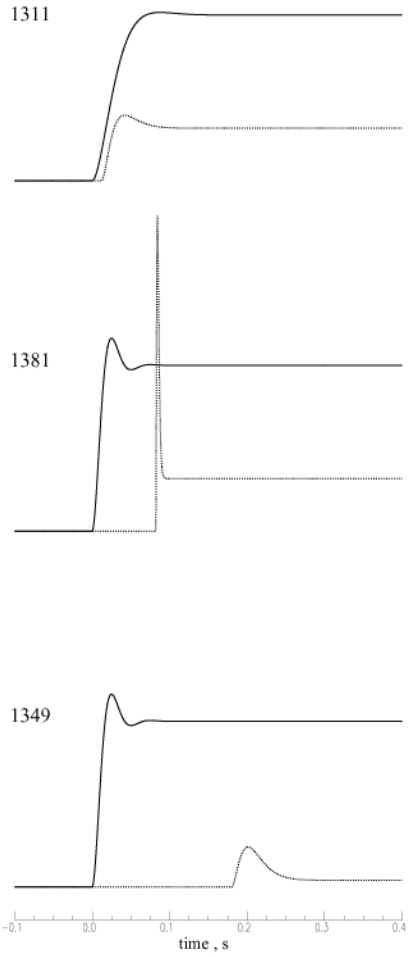

Figure 3. Displacement source functions for the monopole (solid line; after Denny, 1998)) and CLVD (dotted). The CLVD time histories are delayed and their static levels scaled relative to those of the monopole based on the results of this study.

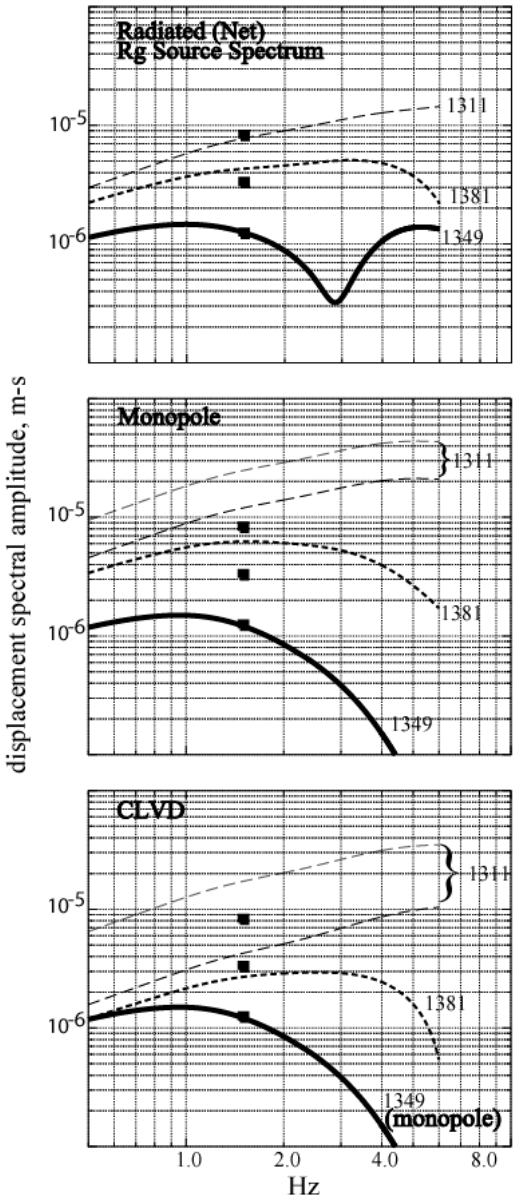

Figure 4. Synthetic *Rg* amplitude spectra for (Top) the final source models, (Middle) monopole sources and (Bottom) CLVD sources. Two spectra are shown for 1311 in the Middle and Bottom panels, one for K=1000 (gray dashed line) and the other for K=100 (black dashed line). Black squares are relative amplitudes based on m_b(*Lg*) values. *Lg* amplitudes were normalized to the *Rg* source spectrum for 1349 at 1.5 Hz (the frequency used to measure the magnitude).

Quantifying the Effects of Confinement on Explosion-Generated *Rg*: Preliminary Results from a New Dataset (Hooper, Bonner, and Leidig)

During the summer of 2003, the Source Phenomenology Experiment was conducted to investigate the differences between confined single-fired chemical explosions (surrogates for nuclear tests) and unconfined delay-fired mining explosions. As part of this experiment, nine single-fired chemical shots were designed, detonated, and recorded in an active pit at a mine in Arizona. The data acquired during the experiment have allowed us to further examine the excitation of *Rg* from explosions, specifically in and below a topographic bench at the mine.

Only four of the above-mentioned shots (Shots 6–9) are considered in this paper. All four shots were loaded similarly to typical production shots at the mine. Their source characteristics are tabulated in Table 1. Shots 6 and 7 were detonated in the pit below the bench, while Shots 8 and 9 were detonated in the bench and experienced the effects of the free face. The data used in this study were recorded on a network of 130 vertical single-component seismic stations (Texans), which were set up along roads in the mine at varying azimuths from the SPE shots, and at distances ranging from 1.5 to approximately 13 km. See Leidig *et al*. (2004) in these proceedings for a summary.

Table 1. Origin data for a subset of the Black Mesa SPE shots

Name	Latitude	Longitude	Elev (m)	# Boreholes	Yield (lbs)	Depth (m)	Confinement
SHOT6	36.4583	-110.3053	2046	6	5708	15	Unconfined (in pit below bench)
SHOT7	36.4585	-110.3051	2046	3	3590	15	Unconfined (in pit below bench)
SHOT8	36.4581	-110.3051	2062	6	6094	15	Unconfined (in bench beside free face)
SHOT9	36.4584	-110.3049	2059	3	3290	15	Unconfined (in bench beside free face)

Figure 5 presents video captures of Shots 6 and 8, and demonstrates the surficial effects of detonating an explosion in the bench near the free face (Shot 8, lower plots) as compared with detonating an explosion in the test pit without a free face (Shot 6, upper plots). Both shots had yields of approximately 3 tons, and the video captures show that the vertical movement of the material for both shots is similar. However, we note that there is an additional component of horizontal movement for the explosion on the free face (Shot 8). Similar effects were noted for Shots 7 and 9, which were designed similarly to the blasts shown in Figure 6, but with approximately half the yield (see Table 1). The videographic data for Shot 7 were difficult to interpret due to obstruction of the camera.

Data Analysis The Texan data were processed as follows:

1) *Rg* was extracted from the Texan data using phase match filtering;
2) The data were corrected for geometric spreading and for attenuation to a normalization distance of 6 km, using 1-D velocity and attenuation models;
3) Spectral energies were estimated for both the corrected and uncorrected *Rg* waveforms for 0.5-1 Hz, 1-2 Hz, and 2-4 Hz,
4) Radiation patterns were plotted using both the attenuation-corrected data and uncorrected spectral energy ratios.

Figure 6 shows comparative radiation patterns for Shots 6 and 8 (top) and Shots 7 and 9 (bottom) using corrected spectral energies. The idea was to compare the shots in the bench to the shots in the test pit in order to tease out the effects of the free face. We computed moving averages of the energies and plotted them as solid lines to aid in the radiation pattern interpretation. The data have been corrected for attenuation and geometric spreading. Similar results were obtained using uncorrected data plotted as spectral ratios (Figure 7).

In the upper subplot of Figure 6, we show the comparison of the two ~3 ton explosions, with Shot 6 (gray) detonated in the pit and Shot 8 (black) detonated in the bench next to the free face. All three frequency ranges show the same phenomena. We observe that at azimuths in front of the face (i.e. in the direction of the test pit – the white area) the energies for Shot 8 (bench with free face) are equivalent to the energies of Shot 6 (pit). However, at azimuths behind the face (the gray area), we see a large increase in the energies for Shot 8 (by a factor of 1.5 at azimuths near the bench normal). This is most evident at 0.66 Hz, since the effects of variable attenuation to the east skew the analysis for 1.5 and 3 Hz. However, even with the attenuation model problems at these higher frequencies, it is obvious that the energies are greatly enhanced behind the free face for Shot 8 (bench with free face) at all three frequencies.

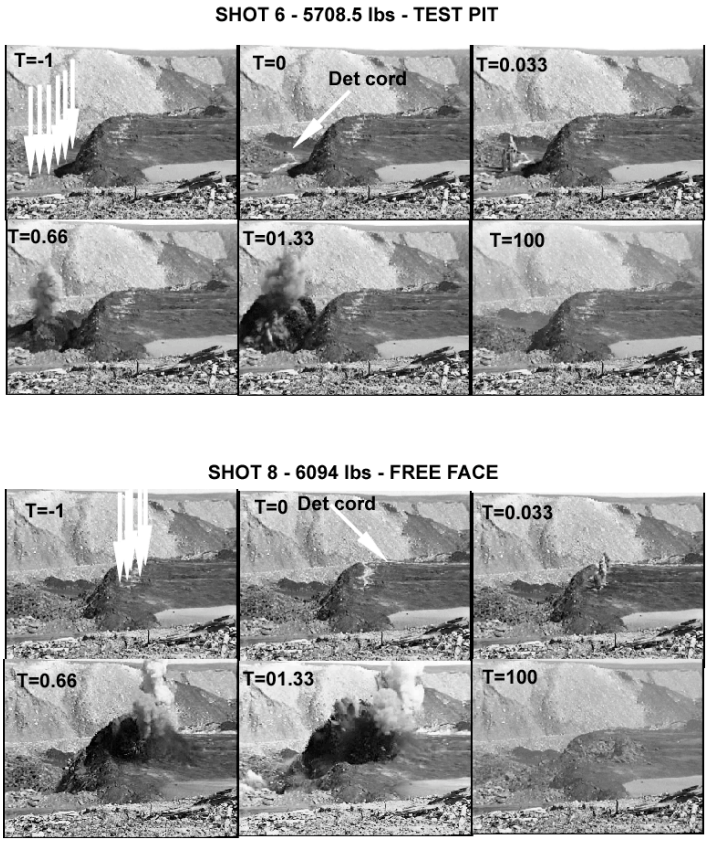

Figure 5. Video capture comparison of Shot 6 (in test pit) and Shot 8 (in bench / on free face).

A similar conclusion can be drawn from the comparison of Shot 7 (pit) and Shot 9 (bench with free face) shown in the lower subplot of Figure 6. In this case, the shots were both ~1.5 tons, detonated at the same depths as Shots 6 and 8. We see a bipolar radiation pattern for Shot 7, which is different from all of the other shots studied. We observe increased energy generation to the SW in this radiation pattern. As mentioned previously, our videographic data for this shot were difficult to interpret due to blockage by the free face and debris from previous blasts. It is possible that this shot did not detonate as designed, given that the alignment of the radiation pattern is parallel to the line of boreholes. When these problems with Shot 7 are taken into account, we see that Shot 9 and Shot 7 had similar energies in front of the free face; however the Shot 9 energies behind the free face are again 1.5 times larger than the energies in front of the free face.

Figure 6 also shows that the radiation patterns change as a function of frequency. This suggests that the explosion sources at Black Mesa (and probably elsewhere) were not simple isotropic explosions. We also note that the scatter in the energies is increased at higher frequencies. This is due to small-scale heterogeneities, and it invalidates the assumption that a 1-D velocity and attenuation model is appropriate at Black Mesa. This is not unexpected, given the geologic setting; however there isn't enough data to develop a 2-D or 3-D attenuation model.

Figure 7 shows plots similar to Figure 6, but using uncorrected data plotted as spectral ratios. The solid lines represent the theoretical Mueller-Murphy spectral ratios for these shots. The left plot presents ratios between the two shots in the pit (Shot 7 / Shot 6), and the two shots on the bench (Shot 9 / Shot 8). Both spectral ratio patterns are close to circular, indicating that the energies of the compared shots are similar. We also see evidence of increased energy generation in the SW quadrant for Shot 7, as discussed earlier. The right plot presents ratios between the shots in the pit and the shots on the bench (Shot 8 / Shot 6 and Shot 9 / Shot 7). These ratios are decidedly not circular, indicating that the energies of the compared shots are not similar. For azimuths in the SW and NW quadrants, the observed ratios are very close to the theoretical ratios (~1). However, for azimuths in the NE and SE quadrants, the observed ratios are increased to greater than 1.5. Given that the approximate bench azimuth is NNE-SSW, the changes in these ratio patterns suggest that the free face is playing an important role in determining the *Rg* radiation patterns for these shots. These results, combined with the results shown in Figure 6, suggest that the *Rg* energies from shots fired on the bench are increased at azimuths behind the free face.

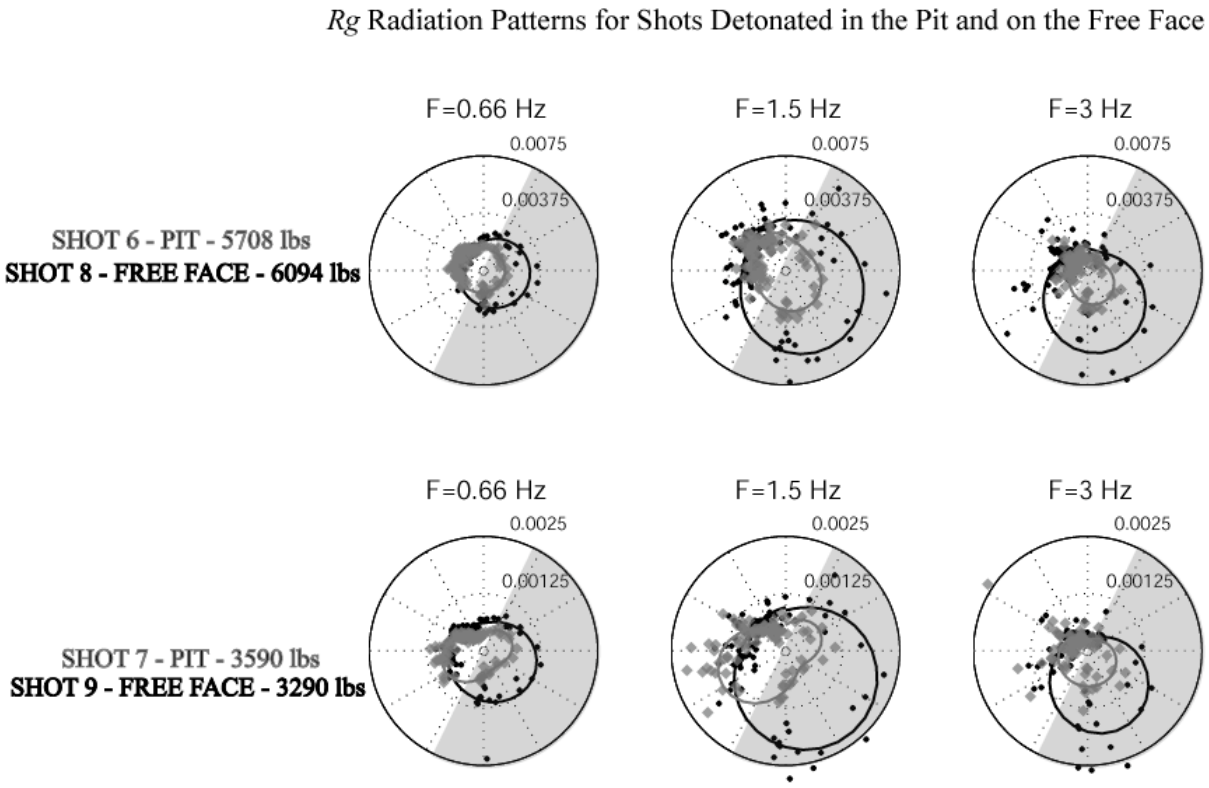

Figure 6. Azimuthal variations in *Rg* energy at 0.66 Hz (left), 1.5 Hz (middle) and 3 Hz (right) for Shots 6 and 8 (top) and Shots 7 and 9 (bottom). The white side of the circle is the pit, while the gray side is the bench. The line between white and gray shows the orientation of the free face.

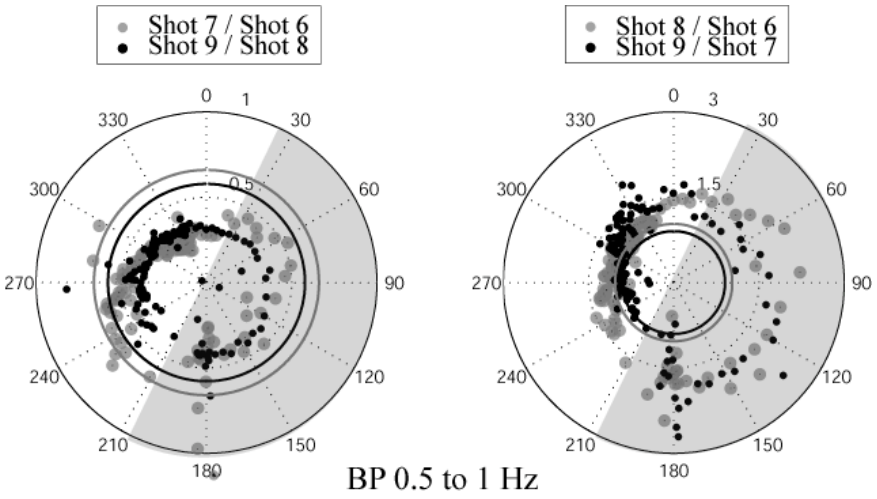

Figure 7. Station-based spectral ratios for combinations of Shots 6-9 in the bandwidth of 0.5 to 1 Hz. The gray and black circles represent the theoretical ratios based on Mueller and Murphy (1971) sources. The white side of the circle is the pit, while the gray side is the bench. The line between white and gray shows the orientation of the free face.

CONCLUSIONS AND RECOMMENDATIONS

Short-period surface waves generated by explosions contain important information about the properties of seismic sources. In the two research projects presented here, we show that a pure monopole source cannot model observed surface waves from chemical explosions at the Shagan Test Site and an Arizona coal mine. For the former, a combined monopole and CLVD source is required to model the surface wave phase and energy data, while for the latter, the effects of lack of confinement, horizontal spall, and non-linear free-face effects contribute to the observed anisotropic radiation patterns. In future research, we will seek to create more complicated models for these sources, in the hope of improving our understanding of the physical phenomena associated with small explosions.

REFERENCES

Bonner, J. L., D. C. Pearson, W. S. Phillips, and S. R. Taylor (2001), Shallow Velocity Structure at the Shagan River Test Site in Kazakhstan, *Pure Appl. Geophys*. 158, 2017-2039.

Bonner, J. L., H. Patton, A. Rosca, H. Hooper, J. Orrey, M. Leidig, and I. Gupta (2003), Aspects of *Rg* and *Lg* Generation from the Shagan Depth of Burial Explosions, in *Proceedings of the 25th Seismic Research Review - Nuclear Explosion Monitoring: Building the Knowledge Base*, LA-UR-03-6029, Vol. 1, 384-393.

Day, S. M. and K. McLaughlin (1991), Seismic Source Representation for Spall, *Bull. Seism. Soc. Am*. 81,191-201.

Denny, M. D. (1998), Seismic-source Corner Frequencies from the Depth of Burial Experiment, University of California, *LLNL Report No. UCRL-ID-132296*.

Denny, M. D. and L. R. Johnson (1991), The Explosion Seismic Source Function: Models and Scaling Laws Reviewed, in *Explosion Source Phenomenology*, Am. Geophys. Monograph 65, 1-24.

Dziewonski, A., S. Bloch and M. Landisman (1969), A Technique for the Analysis of Transient Seismic Signals,

Glenn, L. A. and S. C. Myers (1997), Depth of Burial Experiments at Balapan, University of California, *LLNL Report No. UCRL-ID- 128313*.

Gupta, I. N., W. W. Chan, and R. A. Wagner (1992), A Comparison of Regional Phases from Underground Nuclear Explosions at East Kazakh and Nevada Test Site, *Bull. Seismol. Soc. Am*. 82, 352-382.

Gupta, I. N., T. R. Zhang, and R. A. Wagner (1997), Low-frequency *Lg* from NTS and Kazakh Nuclear Explosions - Observations and Interpretation, *Bull. Seism. Soc. Am.* 87, 1115-1125.

Knopoff, L. and M. J. Randall (1970), The Compensated Linear-Vector Dipole: A Possible Mechanism for Deep Earthquakes, *J. Geophys. Res*. 75, 4957-4963.

Landisman, M., A. Dziewonski, and Y. Sato (1969), Recent Improvements in the Analysis of Surface Wave Observations, *Geophys. J. R. Astron. Soc*. 17, 369-403.

Leidig, M., J. Bonner, and H. Hooper (2004), Development of Velocity and Attenuation Models for Black Mesa and Eastern Arizona. *Weston Geophysical Corporation Technical Report, 29p.*

Masse, R. P. (1981), Review of Seismic Source Models for Underground Nuclear Explosions, *Bull. Seism. Soc. Am.* 71, 1249-1268.

Mueller, R.A. and J.R. Murphy (1971), Seismic Characteristics of Underground Nuclear Detonations, *Bull. Seism. Soc. Am.*, 61, 1675-1692.

Myers, S. C., W. R. Walter, K. Mayeda, and L. Glenn (1999), Observations in Support of *Rg* Scattering as a Source for Explosion *S W*aves: Regional and Local Recordings of the 1997 Kazakhstan Depth of Burial Experiment, *Bull. Seism. Soc. Am.* 89, 544-549.

Patton, H. J. and S. R. Taylor (1995), Analysis of *Lg S*pectral Ratios from NTS Explosions: Implications for the Source Mechanism of Spall and the Generation of *Lg* Waves, *Bull. Seism. Soc. Am.* 85, 220-236.

Patton, H. (2004), *Rg* Excitation by Underground Explosions: Insights from the Balapan DOB Experiment. *Weston Geophysical Corporation Final Report. DE-FG02-00ER83123.*

Pearson, D. C., L. A. Glenn, M. D. Denny, and W. S. Phillips (1997), The Source Depth of Burial Experiment at Shagan River, Kazakhstan, Ext. Abstr., University of California, *LLNL Report No. UCRL-JC-131190*.

Saito, M. (1967), Excitation of Free Oscillations and Surface Waves by a Point Source in a Vertically Heterogeneous Earth, *J. Geophys. Res*. 72, 3689-3699.

Stump, B. W. (1985), Constraints on Explosive Sources with Spall from Near-Source Waveforms, *Bull. Seism. Soc. Am.* 75, 361-377.

von Seggern, D. and R. Blandford (1972), Source Time Functions and Spectra for Underground Nuclear Explosions, *Geophys. J. R. Astron. Soc*. 31, 83-97.